

### Research Article

# Molecular Insights on the Interactions of Nitrosamines from Cigarette Smoking with CYP2A13 using Molecular Docking and Molecular Dynamics Simulation

Jorddy N Cruz<sup>1,2\*</sup>, Mozaniel S Oliveira<sup>3</sup>, João H Vogado<sup>1</sup>, Sebastião G Silva<sup>3</sup>, Wanessa A Costa<sup>3</sup>, Fernanda WF Bezerra<sup>3</sup>, Renato A Costa<sup>4</sup>, Raul NC Junior<sup>3</sup> and Antonio MJC Neto<sup>2</sup>

<sup>1</sup>Faculty of Pharmaceutical Sciences, University of the Amazon, Avenida Alcindo Cacela, Belém, Brazil

<sup>2</sup>Laboratory of Preparation and Computation of Nanomaterials, Federal University of Para, Belém, Brazil

<sup>3</sup>Faculty of Food Engineering, Federal University of Para, Belém, Brazil

<sup>4</sup>Faculty of Chemistry, Federal University of Para, Belém, Brazil

## Abstract

In this work we have studied the molecular interactions of N'-Nitrosoanabasine (NAB) and N'-Nitrosoanatabine (NAT) with CYP2A13 by means of molecular docking simulations. For a more in depth analysis of the dynamics of CYP-ligand interaction we performed molecular dynamics simulations in a total time of 100ns. The results of our Root Mean Square Deviation (RMSD) study revealed that the backbone of the enzyme remained balanced and the ligands underwent small conformational changes. Throughout the simulation time the binders remained at their binding sites. The obtained binding free energy values demonstrated that the formation of the complexes was spontaneous. The values obtained were as follows,

\*Corresponding author: Jorddy Neves Cruz, Faculty of Pharmaceutical Sciences, University of the Amazon, Belém, Brazil, Tel: +55 66065219; Email: jorddynevescruz@gmail.com

**Citation:** Cruz JN, Oliveira MS, Vogado JH, Silva SG, Costa WA, et al., (2018) Molecular Insights on the Interactions of Nitrosamines from Cigarette Smoking with Cyp2a13 using Molecular Docking and Molecular Dynamics Simulation. J Pulm Med Respir Res 4: 018.

**Received:** July 14, 2018; **Accepted:** August 06, 2018; **Published:** August 21, 2018

**Copyright:** © 2018 Cruz JN, et al., This is an open-access article distributed under the terms of the Creative Commons Attribution License, which permits unrestricted use, distribution, and reproduction in any medium, provided the original author and source are credited.

CYP-NAB: -38.19 kcal/mol and NAT: -31.08 kcal/mol. The analysis of the energetic components involved in the calculation of free energy showed that the van der Waals interactions and the electrostatic interactions of the gas phase favored the free energy of the complexes.

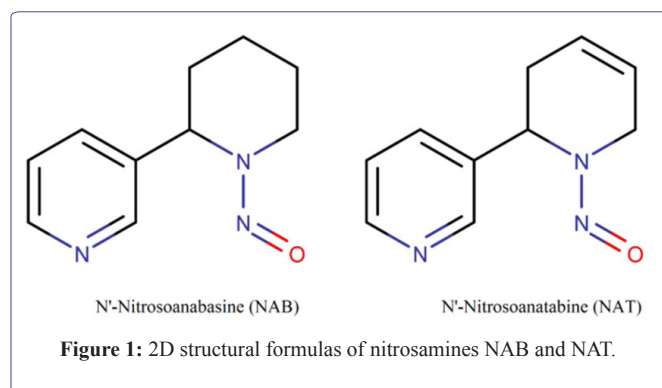
**Keywords:** CYP2A13; Lung cancer; Molecular interactions; Nitrosamines; Tobacco

## Introduction

Cigarette smoking continues to be one of the leading causes of death and disease worldwide. In the United States alone, approximately 433,000 adults die each year from smoking related diseases, causing medical expenses of up to \$100 billion [1]. In Brazil, tobacco consumption is still very high, especially among young students [2]. However, worldwide statistics show that the number of smokers has fallen, mainly between the years 1980 and 2012 [3,4]. One of the consequences of smoking is the various lung diseases that its chemical components can cause, for example chronic bronchitis, chronic obstructive pulmonary disease, obstruction of small airways, emphysema and pulmonary hypertension [1].

Another serious illness that affects most smokers is cancer [5], especially lung cancer. This disease may be associated with high frequency of cigarette smoking as well as its prolonged use during life [6,7]. Increased incidences of lung cancer have been reported since the 1930s, and by 2012 it was estimated to have been responsible for the death of approximately 1,590,000 people. It remains one of leading causes for cancer deaths globally. Among men, the deaths occur mainly in Central and Eastern Europe and among women in North America, Northern Europe, Eastern Asia, Western Europe, Oceania and the Caribbean [8,9]. Overall, the mortality rate due to lung cancer is the highest in countries where people start smoking earlier, such as in North America and Europe [10].

Figure 1 shows the chemical compounds N'-Nitrosoanabasine (NAB) and N'-Nitrosoanatabine (NAT) formed from anabasine and anatabine, respectively [11]. One of the likely causes of lung cancer is the nitrosamines derived from tobacco smoke [12].



The molecules present in tobacco and tobacco smoke begin to act in the body only after enzymatic activation that can be achieved by cytochrome P450 2A13 (P450 or CYP) and is considered a key reaction pathway for initiation of bioactivation of carcinogenesis, and consequently of the progressive changes in the biological profile of the cell [13,14].

A useful tool to demonstrate interactions between nitrosamine linkers and CYP2A catalytic sites is the molecular docking study, which comprises the mechanism of activation and/or oxidation of substrates that may aid in the development of new drugs. In this sense, the present study aims to demonstrate the mechanism of interaction for the activation of NAB and NAT molecules by cytochrome P450 2A13 [15,16].

In this paper, we have described the molecular docking results of NAB and NAT ligands interaction with cytochrome P450 2A13. We also performed Molecular Dynamics (MD) simulation to evaluate the intermolecular interactions during the period of the simulation. Finally, we studied the spontaneity of the formation of the systems and their energetic components by means of free energy calculations using the Molecular Mechanics/Generalized-Born Surface Area (MM/GBSA) methods.

## Materials and Methods

### Molecular docking

The chemical structures of the NAB and NAT were designed using the GaussView software and then optimized with the DFT method at the B3LYP [17,18] using the Gaussian 09 software [19].

Molecular docking studies were performed using the software Molegro Virtual Docker 5.5 (MVD 5.5) [20]. The crystallographic structure of cytochrome P450 2A13, used as a receptor, can be located in the Protein Data Bank (PDB) with ID: 4EJG [16]. The MolDock scoring function (GRID) was used with a grid resolution of 0.30 Å and a radius of 6 Å encompassing the entire bond cavity.

### Molecular dynamics simulation

Every inhibitor atom had its atomic charge calculated using the Restrained Electrostatic Potential (RESP) from the HF/6-31G\* basis set [21-23]. The protonation state of each protein residue was determined using the PDB2PQR server [24].

The protein inhibitor system was constructed for the simulation using the tleap modulus of AMBER 16 [25,26]. The General Amber Force Field (GAFF) [27] and ff14SB [28] force field was used for all the solvent-solvent simulations with the TIP3P [29] model water molecules. The system was solvated in a truncated octahedron periodic box. The cut-off radius was 12 Å for all solvent atoms relative to the solute in the x, y and z axes and a suitable number of counter-ions were added to the system to neutralize their charge.

Energy minimization was performed in the AMBER 16 sander module. At each stage, 5000 cycles were performed using the steepest descent method and conjugate gradient algorithm. In the first, the protein and inhibitor were fixed by applying a harmonic force constant of 200 kcalmol<sup>-1</sup>Å<sup>-2</sup>, the water molecules being free to move. In the following two, the restraint strength was reduced, so that in the final stage the entire system would be able to move freely.

After minimization, the systems were gradually heated from 0 to 300k in five steps, for a total time of 600ps. In four of these, a constant force harmonic of 25kcalmol<sup>-1</sup>Å<sup>-2</sup> was used to restrict heavy atoms. In the final step, the restraining force was reduced to zero so that the whole solute was free to move. These stages were performed using the Langevin thermostat [30] with a collision frequency of 3.0 ps<sup>-1</sup>.

Following this, in order to obtain system equilibrium, a simulation of 2ns was performed at a temperature of 300k, with constant pressure without restriction. The calculation of the electrostatic interactions was performed using the Particle Mesh Ewald method [31] and the SHAKE [32] algorithm was utilized to restrict the bond lengths involving the hydrogen atoms. Afterward, molecular dynamics simulations of production up to 100ns were performed for all systems, unrestrained in the NVT ensemble.

### Free energy calculation

The binding free energies were calculated using the MM/GBSA [33,34] method implemented in the AMBER 16. For each system, 500 snapshots of the last 5ns were used on the MD trajectory. For each snapshot, free energy is calculated for the protein, ligand, and complex using a single trajectory approach. The binding free energy was computed as the difference:

$$\Delta G_{\text{bind}} = G_{\text{complex}} - G_{\text{receptor}} - G_{\text{ligand}} \quad (1)$$

$$\Delta G_{\text{bind}} = \Delta H - T\Delta S = E_{\text{MM}} + \Delta G_{\text{solv}} - T\Delta S \quad (2)$$

$$\Delta E_{\text{MM}} = \Delta E_{\text{internal}} + \Delta E_{\text{electrostatic}} + \Delta E_{\text{vdW}} \quad (3)$$

$$\Delta G_{\text{solv}} = \Delta G_{\text{GB}} + \Delta G_{\text{nonpol}} \quad (4)$$

In which  $\Delta G_{\text{bind}}$  is the free energy of the protein-ligand binding, resulting from the sum of the molecular mechanics energy ( $\Delta E_{\text{MM}}$ ), the desolvation free energy ( $\Delta G_{\text{solv}}$ ), and the entropy ( $-T\Delta S$ ). The energy of molecular gas phase mechanics ( $\Delta E_{\text{MM}}$ ) can be described by the sum of the internal energy contributions ( $\Delta E_{\text{internal}}$ ), the sum of the connection, angle and dihedral energies), electrostatic contributions ( $\Delta E_{\text{electrostatic}}$ ) and van der Waals terms ( $\Delta E_{\text{vdW}}$ ). Desolvation free energy ( $\Delta G_{\text{solv}}$ ) is the sum of the polar ( $\Delta G_{\text{GB}}$ ) and non-polar ( $\Delta G_{\text{nonpol}}$ ) contributions. The polar desolvation term was calculated using the implicit Generalized Born (GB) approaches.

## Results and Discussion

For studying the interactions between NAB and NAT molecules with CYP450 2A13, the molecular docking simulation at the cytochrome binding site was performed. This site has a surface area of 166.40 Å<sup>2</sup>, volume 67.58 Å<sup>3</sup> and position x: 22.55, y: -11.51 and z: 37.43 for accommodation of the molecules (Figure 2).

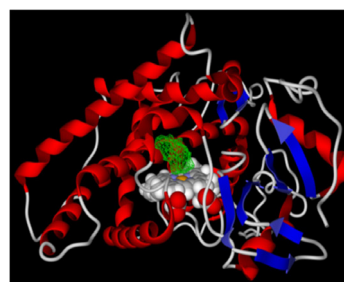


**Figure 2:** The binding pocket of the molecules is represented by green color.

This cytochrome was chosen because it is expressed in the respiratory tract [35] and is responsible for the metabolism of nitrosamines [36].

The molecular docking simulation of these nitrosamines with cytochrome was performed because NAB [37] and NAT [38] are carcinogenic agents present in tobacco smoke. In several studies they have been reported as being responsible for causing lung cancer [39-41]. Therefore, elucidation of the binding mechanism of these molecules is important for the study of their metabolism. The molecular docking results are summarized in table 1.

The MolDock score found for NAB (-86.74) and NAT (-82.86) at the P450 binding site was favorable for the ligand receptor interaction, as it favored the molecular stability of the system. In addition, the affinity values for the binding of the molecules to the cytochrome were favorable, demonstrating that these compounds were capable of binding to cytochrome to perform productive interactions. For NAB and NAT, these values were -97,963 kcal/mol and -99,803 kcal/mol respectively. The energy contribution of the HEME prosthetic group was also calculated and its values were found favorable in both the systems. The energy contribution for the molecules NAB and NAT were -17.281 kcal/mol and -11.036 kcal/mol respectively.

With the above obtained results it became possible to verify the interactions between the molecules and the residues of the protein and the HEME prosthetic group.

These interactions are described in the following tables 2 and 3 and figure 3a and 3b.

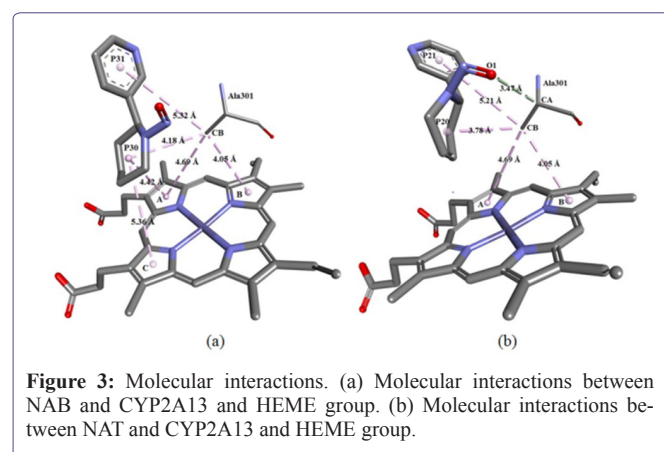


**Figure 3:** Molecular interactions. (a) Molecular interactions between NAB and CYP2A13 and HEME group. (b) Molecular interactions between NAT and CYP2A13 and HEME group.

Molecules	MolDock Score <sup>a</sup>	Rerank Score <sup>b</sup>	Interaction (kcal/mol) <sup>c</sup>	Contribution of the Cofactor <sup>d</sup>	Internal <sup>e</sup>	LE1 <sup>f</sup>	LE3 <sup>g</sup>
NAB	-86.74	-72.07	-97.96	-17.28	11.22	-6.19	-5.14
NAT	-82.86	-71.82	-99.8	-11.03	16.93	-5.91	-5.12

**Table 1:** Molecular docking results.

**Note:** <sup>a</sup>The scoring function used by MolDock is derived from the PLP score and has a new term for hydrogen bonds and new charge methods [20]

<sup>b</sup>Rerank Score is a linear combination of E-inter (stereo, van der Waals, hydrogen bonding and electrostatic) between the binder and the protein, and E-intra (torsion, sp<sup>2</sup>-sp<sup>2</sup>, hydrogen bonding, van der Waals and electrostatic) of the binder corrected by pre-defined coefficients [20]

<sup>c</sup>Energy of the total interaction between the pose and the protein

<sup>d</sup>Energy of interaction between the pose and the prosthetic group

<sup>e</sup>Energy of the pose

<sup>f</sup>MolDock Score divided by the count of the heavy atoms

<sup>g</sup>Rerank score divided by the count of the heavy atoms

Molecule	Residue	Group Heme	Interaction	Distance (Å)
P30	Ala301-CB	-	Hydrophobic: Alkyl	4.18
P31	Ala301-CB	-	Hydrophobic: Pi-Alkyl	5.32
-	Ala301-CB	B	Hydrophobic: Pi-Alkyl	4.05
-	Ala301-CB	A	Hydrophobic: Pi-Alkyl	4.69
P30	-	A	Hydrophobic: Pi-Alkyl	4.42
P30	-	C	Hydrophobic: Pi-Alkyl	5.36

**Table 2:** Interactions performed by NAB with CYP2A13 and with the HEME group.

Molecule	Residue	Group Heme	Interaction	Distance (Å)
O1	Ala301-CA	-	Hydrogen Bond	3.47
P20	Ala301-CB	-	Hydrophobic: Alkyl	3.78
P21	Ala301-CB	-	Hydrophobic: Pi-Alkyl	5.21
-	Ala301-CB	A	Hydrophobic: Pi-Alkyl	4.69
-	Ala301-CB	B	Hydrophobic: Pi-Alkyl	4.05

**Table 3:** Interactions performed by the NAT with CYP2A13 and with the HEME group.

The value of binding affinity energy for the NAB compound was found to be -97,963 kcal/mol. The Pyridine ring (P31) interacted with the CB atom of alanine 301, at a distance of 5.32 Å through a hydrophobic pi-alkyl interaction. The same alanine atom interacted with the Piperidine ring (P30) at a distance of 4.18 Å by means of an alkyl interaction. The piperidine ring interacted with the pyrrole rings A and C of the HEME prosthetic group via hydrophobic pi-alkyl interactions at the distances of 4.42 and 5.36 Å, respectively. The alanine residue also interacted with the HEME group via hydrophobic pi-alkyl interactions with its pyrrole rings A and B at the distances of 4.69 and 4.05 Å, respectively.

The NAT molecule, having an interaction energy value of -99.803 kcal/mol, showed the best interaction with the active site of the protein in the docking simulation. This molecule showed three interactions with the alanine residue. The atom O1 of the molecule interacted with the CA atom of alanine 301 by means of hydrogen bonding at a distance of 3.47 Å. In this interaction the NAT molecule is the acceptor and the alanine molecule is the donor of the hydrogen atom. The CB atom interacted with the P21 ring by means of a pi-alkyl interaction at a distance of 5.21 Å while it interacted with the Pyridine ring (P20) through an alkyl interaction at a distance of 3.78 Å. The pyrrole rings A and B of the HEME group interacted with the alanine residue by means of hydrophobic pi-alkyl type interaction at the distances of 4.69 and 4.05 Å, respectively.

### Analysis of the stability of the three-dimensional structure of protein and ligands

In molecular docking simulations, with the Mocker Virtual Docker, the protein is considered rigid and the binder flexible [20]. Thus, the molecular dynamics simulation was adopted to refine the results obtained for the cytochrome interaction with the NAB and NAT ligands. In addition, the stability of the systems was also analyzed. For this analysis the Root Mean Square Deviation (RMSD) value was used in relation to the starting structure (minimized, heated and balanced) for molecular dynamics simulation. The RMSD results for the systems over a total time of 100 nanoseconds are shown in figure 4.

The mean values obtained for the RMSD of the alpha carbon of the protein backbone were as follows, CYP-NAB: 1.03 Å and CYP-NAT: 1.14 Å. These values demonstrated that the protein structure during the molecular dynamics simulation did not deviate significantly from its initial conformation.

Throughout the simulation of the NAT its structural conformation underwent changes alternating its state between moments of molecular balance and small conformational variations. The NAB molecule also maintained its equilibrium at the CYP site, undergoing small conformational changes during the simulation. Throughout the simulation time the NAB and NAT compounds remained bound to the CYP binding pocket.

### Analysis of free energy and its components

To obtain the values of the binding free energy components of all the ligands interacting with CYP, we used the MM/GBSA methods [33-35]. The results obtained are summarized in table 4.

According to the values obtained with the free energy calculations, the binders showed the following bond affinity values: CYP-NAB: -38.19 and CYP-NAT: -31.08.

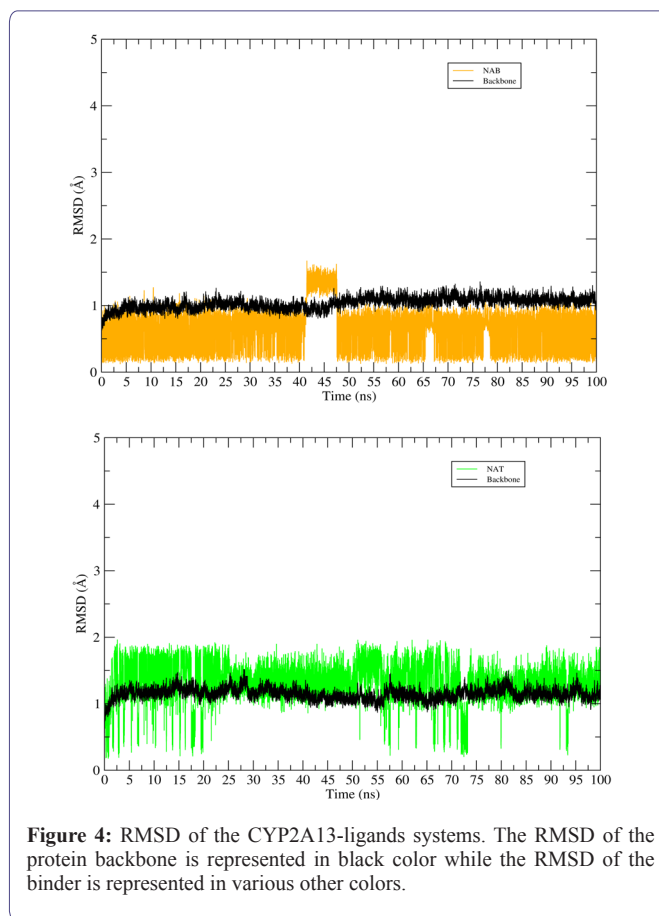


Figure 4: RMSD of the CYP2A13-ligands systems. The RMSD of the protein backbone is represented in black color while the RMSD of the binder is represented in various other colors.

In addition to the absolute values of free energy, its components were also calculated so that the mechanism of interaction of the molecules with the protein is better understood. In all the systems the van de Waals interactions ( $\Delta E_{vdw}$ ) and the electrostatic interactions of the gas phase ( $\Delta E_{ele}$ ) favored the bond free energy ( $\Delta G_{bind}$ ) of the complexes. The values for nonpolar solvation energies ( $\Delta G_{npol,sol}$ ) and the non-polar ( $\Delta E_{non-polar}$ ) contributions were similar to each other and also favored the ligand receptor interaction.

### Conclusion

Our molecular docking results demonstrated that the major interactions that occurred between the NAB and NAT molecules and the enzyme and the HEME group were hydrophobic in nature. During the entire period of simulation, the ligands continued to interact with the CYP, undergoing some conformational changes. Our MM/GBSA results demonstrated that the formation of the complexes was spontaneous and the values obtained for  $\Delta G_{bind}$  were as follows: CYP-NAB: -38.19 kcal/mol and NAT: -31.08 kcal/mol. For the complexes the van de Waals ( $\Delta E_{vdw}$ ) interactions and the electrostatic interactions of the gas phase ( $\Delta E_{ele}$ ) favored the bonding energy ( $\Delta G_{bind}$ ). The values for nonpolar solvation energies ( $\Delta G_{npol,sol}$ ) and the non-polar ( $\Delta E_{non-polar}$ ) contributions were similar to each other and also favored the ligand-receptor interaction. With our results it was possible to understand the mechanism of interaction of NAB and NAT that after being metabolized by CYP2A13 will form DNA adducts capable of inducing lung cancer.



Ligand	$\Delta E_{vdw}$	$\Delta E_{ele}$	$\Delta G_{ele,sol}$	$\Delta G_{npot,sol}$	$\Delta E_{non-polar}$	$\Delta E_{polar}$	$\Delta G_{bind}$
NAB	-34.97 ± 0.04	-9.50 ± 0.05	10.31 ± 0.02	-4.02 ± 0.01	-38.99	1.07	-38.19 ± 0.05
NAT	-31.78 ± 0.04	-7.92 ± 0.05	12.62 ± 0.03	-4.01 ± 0.01	-35.79	4.70	-31.08 ± 0.05

**Table 4:** Binding free energy and its components.

## Acknowledgment

Jorddy N. Cruz and Antonio M. J. C. Neto appreciate the support of the Federal University of Pará and the National Council for Scientific and Technological Development (CNPq). Oliveira M. S (Process Number: 1662230), Costa W. A. (Process Number: 1427204) and Bezerra F. W. F. (Process Number: 1718822) thank CAPES for the doctorate scholarship.

**Conflict of Interest:** The authors declare that there are no conflicts of interest regarding the publication of this paper.

**Ethical Approval:** The present work was approved by the Ethics Council of the Federal University of Pará

## Disclosure

J.N. Cruz is the principle author. The study includes no identifiable information.

## Author's Contributions

All authors contributed equally to the development of this article.

## References

- US Department of Health and Human Services (2010) How Tobacco Smoke Causes Disease: The Biology and Behavioral Basis for Smoking-Attributable Disease. US Department of Health and Human Services, Washington D.C., USA.
- Pinheiro MDA, Torres LF, Bezerra MS, Cavalcante RC, Alencar RD, et al. (2017) Prevalence and associated factors of alcohol consumption and smoking among medical students in northeastern Brazil. *Rev Bras Educ Med* 41: 231-239.
- Ng M, Freeman MK, Fleming TD, Robinson M, Dwyer-Lindgren L, et al. (2014) Smoking prevalence and cigarette consumption in 187 countries, 1980-2012. *JAMA* 311: 183-192.
- Frieden TR, Jaffe HW, Richards CL, Iademarco MF, Cono J (2014) Current cigarette smoking among adults-United States, 2005-2012. *Centers for Disease Control and Prevention, Morbidity and Mortality Weekly Report* 63: 29-34.
- Pesch B, Kendzia B, Gustavsson P, Jöckel KH, Johnen G, et al. (2012) Cigarette smoking and lung cancer--relative risk estimates for the major histological types from a pooled analysis of case-control studies. *Int J Cancer* 131: 1210-1219.
- Barrera R, Shi W, Amar D, Thaler HT, Gabovich N, et al. (2005) Smoking and timing of cessation: Impact on pulmonary complications after thoracotomy. *Chest* 127: 1977-1983.
- Clifford GM, Lise M, Franceschi S, Egger M, Bouchardy C, et al. (2012) Lung cancer in the Swiss HIV cohort study: Role of smoking, immunodeficiency and pulmonary infection. *Br J Cancer* 106: 447-452.
- Mao Y, Yang D, He J, Krasna MJ (2016) Epidemiology of Lung Cancer. *Surg Oncol Clin N Am* 25: 439-445.
- Islami F, Torre LA, Jemal A (2015) Global trends of lung cancer mortality and smoking prevalence. *Transl Lung Cancer Res* 4: 327-338.
- Ahmad A, Gadgeel S (2016) Lung Cancer and Personalized Medicine, Springer International Publishing, Cham, Switzerland.
- Hoffmann D, Hecht SS (1985) Nicotine-derived N-nitrosamines and tobacco-related cancer: Current status and future directions. *Cancer Res* 45: 935-944.
- Ramírez N, Özel MZ, Lewis AC, Marcé RM, Borrull F, et al. (2014) Exposure to nitrosamines in thirdhand tobacco smoke increases cancer risk in non-smokers. *Environ Int* 71: 139-147.
- Wong HL, Zhang X, Zhang QY, Gu J, Ding X, et al. (2005) Metabolic activation of the tobacco carcinogen 4-(methylnitrosamino)-(3-pyridyl)-1-butanone by cytochrome P450 2A13 in human fetal nasal microsomes. *Chem Res Toxicol* 18: 913-918.
- Shimada T (2017) Inhibition of carcinogen-activating cytochrome P450 enzymes by xenobiotic chemicals in relation to antimutagenicity and anticarcinogenicity. *Toxicol Res* 33: 79-96.
- Schlicht KE, Berg JZ, Murphy SE (2009) Effect of CYP2A13 active site mutation N297A on metabolism of coumarin and tobacco-specific nitrosamines. *Drug Metab Dispos* 37: 665-671.
- DeVore NM, Scott EE (2012) Nicotine and 4-(methylnitrosamino)-1-(3-pyridyl)-1-butanone binding and access channel in human cytochrome P450 2A6 and 2A13 enzymes. *J Biol Chem* 287: 26576-26585.
- Becke AD (1993) Density-functional thermochemistry. III. The role of exact exchange. *J Chem Phys* 98: 5648-5652.
- Lee C, Yang W, Parr RG (1988) Development of the colle-salvetti correlation-energy formula into a functional of the electron density. *Phys Rev B Condens Matter* 37: 785-789.
- Frisch MJ, Trucks GW, Schlegel HB, Scuseria GE, Robb MA, et al. (2009) Electronic Supplementary Material (ESI) for Chemical Science. The Royal Society of Chemistry 1-20.
- Thomsen R, Christensen MH (2006) MolDock: A new technique for high-accuracy molecular docking. *J Med Chem* 49: 3315-3321.
- Bayly CI, Cieplak P, Cornell W, Kollman PA (1993) A well-behaved electrostatic potential based method using charge restraints for deriving atomic charges: The RESP model. *J Phys Chem* 97: 10269-10280.
- Cornell WD, Cieplak P, Bayly CI, Kollman PA (1993) Application of RESP charges to calculate conformational energies, hydrogen bond energies, and free energies of solvation. *J Am Chem Soc* 115: 9620-9631.
- Wang J, Cieplak P, Kollman PA (2000) How well does a Restrained Electrostatic Potential (RESP) model perform in calculating conformational energies of organic and biological molecules? *Journal of Computational Chemistry* 21: 1049-1074.
- Dolinsky TJ, Nielsen JE, McCammon JA, Baker NA (2004) PDB2PQR: An automated pipeline for the setup of poisson-boltzmann electrostatics calculations. *Nucleic Acids Res* 32: 665-667.

25. Case DA, Cheatham TE 3rd, Darden T, Gohlke H, Luo R, et al. (2005) The Amber biomolecular simulation programs. *J Comput Chem* 26: 1668-1688.
26. Cruz JN, Costa JFS, Khayat AS, Kuca K, Barros CAL, et al. (2018) Molecular dynamics simulation and binding free energy studies of novel leads belonging to the benzofuran class inhibitors of mycobacterium tuberculosis polyketide synthase 13. *J Biomol Struct Dyn* 4: 1-12.
27. Wang J, Wolf RM, Caldwell JW, Kollman PA, Case DA (2004) Development and testing of a general amber force field. *J Comput Chem* 25: 1157-1174.
28. Maier JA, Martinez C, Kasavajhala K, Wickstrom L, Hauser KE, et al. (2015) ff14sb: Improving the accuracy of protein side chain and backbone parameters from ff99SB. *J Chem Theory Comput* 11: 3696-3713.
29. Jorgensen WL, Chandrasekhar J, Madura JD, Impey RW, Klein ML (1983) Comparison of simple potential functions for simulating liquid water. *The Journal of Chemical Physics* 79: 926.
30. Izaguirre JA, Catarello DP, Wozniak JM, Skeel RD (2001) Langevin stabilization of molecular dynamics. *J Chem Phys* 114: 2090.
31. Darden T, York D, Pedersen L (1998) Particle mesh Ewald: An  $N \cdot \log(N)$  method for ewald sums in large systems. *J Chem Phys* 98: 10089.
32. Ryckaert JP, Ciccotti G, Berendsen HJC (1977) Numerical integration of the cartesian equations of motion of a system with constraints: Molecular dynamics of n-alkanes. *J Comput Phys* 23: 327-341.
33. Kollman PA, Massova I, Reyes C, Kuhn B, Huo S, et al. (2000) Calculating structures and free energies of complex molecules: Combining molecular mechanics and continuum models. *Acc Chem Res* 33: 889-897.
34. Hou J T, Wang Y, Li Y, Wang W (2011) Assessing the performance of the MM/PBSA and MM/GBSA methods. I. The accuracy of binding free energy calculations based on molecular dynamics simulations. *J Chem Inf Model* 51: 69-82.
35. Chiang HC, Wang CK, Tsou TC (2012) Differential distribution of CYP2A6 and CYP2A13 in the human respiratory tract. *Respiration* 84: 319-326.
36. Jales JR, Hecht SS, Murphy SE (2005) Cytochrome P450 enzymes as catalysts of metabolism of 4-(methylnitrosamino)-1-(3-pyridyl)-1-butanone, a tobacco specific carcinogen. *Chem Res Toxicol* 18: 95-110.
37. Hecht SS, Stepanov I, Carmella SG (2016) Exposure and Metabolic Activation Biomarkers of Carcinogenic Tobacco-Specific Nitrosamines. *Acc Chem Res* 49: 106-114.
38. Xue J, Yang S, Seng S (2014) Mechanisms of Cancer Induction by Tobacco-Specific NNK and NNN. *Cancers (Basel)* 6: 1138-1156.
39. Wong HL, Murphy SE, Hecht SS (2005) Cytochrome P450 2A-catalyzed metabolic activation of structurally similar carcinogenic nitrosamines: N'-nitrosornicotine enantiomers, N-nitrosopiperidine, and N-nitrosopyrrolidine. *Chem Res Toxicol* 18: 61-69.
40. Hecht SS (1998) Biochemistry, biology, and carcinogenicity of tobacco-specific N-nitrosamines. *Chem Res Toxicol* 11: 559-603.
41. Carlson ES, Upadhyaya P, Hecht SS (2016) Evaluation of nitrosamide formation in the cytochrome P450-mediated metabolism of tobacco-specific nitrosamines. *Chem Res Toxicol* 29: 2194-2205.